Metasurface-Enabled Remote Quantum Interference

Pankaj K. Jha[1], Xingjie Ni[1], Chihhui Wu[1], Yuan Wang[1], and Xiang Zhang[1,2,]

[1]*NSF Nanoscale Science and Engineering Center(NSEC),*

3112 Etcheverry Hall, University of California, Berkeley, California 94720, USA

[2]*Materials Science Division, Lawrence Berkeley National Laboratory,*

1 Cyclotron Road Berkeley, California 94720, USA

(Dated: June 2, 2015)

Abstract

Anisotropic quantum vacuum (AQV) opens novel pathways for controlling light-matter interaction in quantum optics, condensed matter physics, etc. Here, we theoretically demonstrate strong AQV over macroscopic distances enabled by judiciously designed array of sub-wavelength-scale nano-antennas -a metasurface. We harness the phase-control ability and the polarization-dependent response of the metasurface to achieve strong anisotropy in the decay rate of a quantum emitter located over distances of hundreds of wavelengths. Such an AQV induces quantum interference among radiative decay channels in an atom with orthogonal transitions. Quantum vacuum engineering with metasurfaces holds promise for exploring new paradigms of long-range light-matter interaction for atom optics, solid-state quantum optics, etc.

Quantum interference (QI) arises from the indistinguishable paths of photons. QI in the spontaneous emission, from nearly degenerate excited states in a multi-level quantum emitter, leads to a variety of remarkable effects such as coherent population trapping[1], efficient quantum photo engine[2], etc. In an isotropic quantum vacuum, QI has a stringent requirement of non-orthogonal transition dipole moments which is rarely met in atomic systems[3–5]. However, by breaking the isotropic nature of the quantum vacuum, one can circumvent such a constraint and achieve QI for orthogonal transitions[6]. For instance, an atom in the vicinity of few tens of nanometers of a metallic surface[7, 8] or embedded in a photonic crystal[9] have been theoretically proposed that may experience an anisotropic quantum vacuum (AQV). Unfortunately in these approaches, both precise positioning[10–12] and optically addressing the atom for quantum applications are challenging in experiments due to near surface interactions such as surface thermal noise, Casmir-Polder force, quenching, and so forth. A strong AQV over remote distances from any material interface is, therefore, imperative but has never been realistically possible[13, 14].

In this Letter, we propose and theoretically demonstrate a long-sought-after solution for experimentally observable QI in atoms over remote distances using an engineered surface -metasurface. We harness the phase-control ability and the polarization-dependent response of a judiciously designed metasurface to tailor the quantum vacuum and induce strong anisotropy for an atom at a macroscopic distance over $100\lambda_0$, where λ_0 is the wavelength in free space. Quantum vacuum engineering with metasurfaces creates unprecedented opportunities for long-range interactions between quantum emitters, solid-state quantum optics, spintronics, and decoherence-free subspace for quantum information transfer.

A quantum emitter, in the vicinity of a metallic interface[15], can strongly interfere with its own spontaneously emitted photon, after reflecting from the surface and display intriguing interference effects[16–18]. For instance, one can design and construct an interface, near which, a quantum emitter displays orientation dependent decay rate which is a manifestation of AQV[19]. With multi-level quantum emitters, such AQV can induce QI among radiative decay channels even if the corresponding dipole moments are orthogonal to each other. One of the most straightforward ways to engineer the quantum vacuum is to place an infinite-size perfect metallic surface (parallel to x-y plane) in the vicinity ($d \ll \lambda_0$) of an x-dipole. This metallic interface forms an out-of-phase image of the x-dipole. The destructive interference between the direct emission and the reflected field results in the suppression of the spontaneous emission. However, this suppression is quickly washed out beyond $d \sim \lambda_0$ due the fading interference between the direct and the reflected fields.

2

By symmetry, the same mirror can also form an out-of-phase image of a y-dipole. This symmetry leads to an isotropic quantum vacuum in the x-y plane parallel to the mirror. On the other hand, by integrating metasurface we can break this in-plane symmetry and induce strong interference even when the quantum emitter is at macroscopic distance.

The metasurfaces have attracted great interest due to their exceptional light-manipulation properties[20–22]. Recent studies have shown that metasurfaces provide higher degree of freedom in molding the flow of light, compared to bulk metamaterials[21]. It can be used to bend the light abnormally in a fairly broad wavelength range[23, 24], enhance optical spin-orbit interaction[25, 26], couple efficiently propagating waves and surface waves[27], create planar optical lenses[28], build ultra-thin holograms[29], enhance nonlinear optical responses in semiconductor hetero-structures[30], perform mathematical operations[31], negative refraction and planar focusing[32]. However, most of the applications to date has mainly focused on classical fields where the average number of photons per mode is large ($n \gg 1$). Here, we show that a prudentially designed metasurface can also be harnessed for non-classical fields, for instance single photon field and enable QI in a multi-level quantum emitter.

It is advantageous to use a metasurface for quantum vacuum engineering. First, metasurface offers greater degree of freedom in shaping polarization dependent wavefront of the fields[21]. Second, the incident and reflected fields propagate through an optically thin layer of sub-wavelength-scale nano-antennas, the absorption loss due to metal is minimal and a strong back action on the quantum emitter can be realized. Third, optically thin and planar structure of the metasurface makes it a promising candidate for micro-optical devices like atom chips[33] to explore long range interaction between trapped atoms.

The schematic illustration of the metasurface-enabled remote AQV is shown in Fig. 1. The metasurface breaks the symmetry of quantum vacuum fluctuations and creates a strong AQV in the vicinity of a distant quantum emitter. This anisotropy manifests itself in the angular dependence of the decay rate of a two-level quantum emitter with transition dipole moment parallel the surface (x-y plane). In general the decay of a two-level quantum emitter, dipole moment in the x-y plane, is given by $\gamma = \gamma_{xx} \cos^2(\varphi) + \gamma_{yy} \sin^2(\varphi)$ where φ is the azimuthal angle. In an isotropic quantum vacuum with no physical boundary the decay of this dipole is isotropic (red dashed line) i.e independent of its orientation φ but in the presence of a metasurface (green solid line) the decay is anisotropic. Such AQV induces QI among the decay channels in a multi-level quantum emitter.

Nano-antennas, which resonate with the incident light, can shift the phase through their reso-

nances for the scattered light. By changing their resonance properties, e.g. shifting the resonant frequency, through the nano-antenna designs, we can effectively control the amount of the phase shifted in the scattered light. It can be intuitively understood as the light being held for some time due to the resonance before it gets re-emitted, which give a finite phase delay. An array of such sub-wavelength-scale nano-antennas, namely a metasurface, collaboratively can mold the wavefront of the scattered light to an arbitrary form. Without loss of generality, we distributed the nano-antennas on a surface in such a way that it acts as a spherical-mirror for a x-dipole while simultaneously serving as a normal mirror for a y-dipole. Polarization dependent response is illustrated in Fig. 2(a) where the x polarized light is reflected back to the source while the y-z polarized light is de-focused. In Fig. 2(b) we have plotted spatial intensity distribution of a dipole located at 3.7 micron from the metasurface with a cross-sectional area of 12μm$\times 12\mu$m. Fig. 2(c,d) show the intensity distribution of the reflected field for an x- and y-dipole (point) source. One of the limitations of previously studied metasurface designs reside in their poor overall efficiency. This can be overcome with gap plasmon-based gradient metasurfaces by integrating a metallic mirror on the back of the nano-antennas and sandwiching a dielectric spacer layer in between them[34, 35]. With proper optimization tool we achieved 81% (normalized to the total field incident on the metasurface) in the reflection efficiency for the constitutional nano-antennas of the metasurface for the x-polarization through our full-wave numerical simulations (see Supplementary Materials[36]). The calculation in this paper is based on this efficiency.

Polarization selective response can be efficiently achieved by adjusting the phase shifts provided by the constitutional nano-antennas. For x-polarization, the required phase shift for a nano-antenna at the coordinate (x_0, y_0) is given by $\phi(x_0, y_0) = \pi + 2k_0\sqrt{r_0^2 + d^2}$, where d is the distance between the quantum emitter and the metasurface, $r_0 = \sqrt{x_0^2 + y_0^2}$, and k_0 is the wave-number in the vacuum. The coordinate of the quantum emitter is (0,0,d). Here we use five different nano-antenna designs of gold bar as the constitutional elements of the metasurface. Each design provides a distinct phase shift for the x-polarization but not the same phase shift for the y-polarization through its anisotropic plasmonic resonances. The designs with required phase shifts are obtained by sweeping over different geometrical parameters, the length and the width of the gold bars, using full-wave finite element simulations. The five designed nano-antennas are shown in Fig. 3(a). When the size (namely l_x and l_y as shown in the left panel of Fig. 3(a)) of nano-antenna changes, the phase shift of the scattered light of the nano-antenna will changed accordingly in the x-polarized incidence. The response of the five nano-antennas covers the phase shift from 0 to 2π

and matches well with the ideal phase shifts required by the constituent nano-antennas such that the necessary spherical phase profile is imprinted by the metasurface. In Fig.3(b) we have plotted two-dimensional distribution of the phase profile required upon the reflection to focus the incident light and compensate the optical path length from a x-dipole to its image, where the height and the color of the surface plot indicates the phase shift.

Fig. 4 shows the calculated radiative decay rate of a two-level quantum emitter above an infinite-sized metasurface versus the distance d/λ_0. The decay rate is obtained by utilizing the ratio between numerically calculated total emitted power from a dipole [42] with and without the presence of a metasurface. For the x-dipole a constant decay rate $\gamma_{xx} \sim 0.6\gamma_0$ can be engineered, while for a y-dipole the decay rate oscillate[42] and quickly goes to the value of $\gamma_{yy} = \gamma_0$ and remains constant thereafter. Thus we can achieve AQV regardless of the distance by optimizing the design for each point along the z axis. The upper limit to the distance between the quantum emitter and the metasurface is fundamentally constrained by the photonic coherence length[14]. For a given design, considering the metasurface as a focusing device which is diffraction limited, the position tolerance for the dipole is in the order of wavelength. Infinitely large metasurface is equivalent to a solid angle of 2π in the perspective of the dipole. Practically, the solid angle can be close to 2π if the metasurface is sufficiently large. For example, for the solid angle of 1.998π, if the dipole is at a distance of $100\lambda_0$, the radius of the metasurface is about $2234\lambda_0$, and the resulting $\gamma_{xx} = 0.62\gamma_0$. If we consider ^{133}Cs as an isolated trapped atom at $100\lambda_0$, where $\lambda_0 = 894$nm (D_1 transition) the radius the metasurface to project 1.998π radian of solid angle is $\sim 2\,$mm.

To see the effect of AQV on a multi-level quantum emitter we will consider a three-level atom in V-configuration, as shown in Fig. 1 (inset). The details of the atomic transitions and equation of motion are given in the Supplemental Material[36]. In an AQV the orthogonal transition ($|a_{1,2}\rangle \rightarrow |b\rangle$) are coupled whose strength is quantified by the cross-damping[6] term $\kappa \sim \wp_{a_1 b} \cdot \Im[\overleftrightarrow{\mathbf{G}}(\mathbf{r}_0, \mathbf{r}_0, \omega_{ab})] \cdot \wp^*_{a_2 b}$ which in terms of the local coordinates takes the form $\kappa = (\gamma_{xx} - \gamma_{yy})/2$. From Fig. (4) we obtain $\gamma_{xx} = 0.6, \gamma_{yy} = 1$ which yields $\kappa = -0.2$. If we consider $d = 20\lambda_0$ where $\lambda_0 = 894$nm, we obtain a significant cross-damping at a distance of $\sim$18-micron from the metasurface. It is worth to mention that by introducing another metasurface above the quantum emitter, the decay rate can be further reduced and the anisotropy can be enhanced. On the other hand with plasmonic, negative-index metamaterial (with losses), or above a photonic crystal the cross damping $\kappa \sim 0$ over such distances.

In Fig. 5(a) we have plotted population of the excited states $|a_{1,2}\rangle$ as a function of normalized

time $\gamma_0 t$ (see Supplementary Material for calculations[36]). In an isotropic quantum vacuum with no physical boundary the atom decays exponentially with a characteristic times constant $\tau_c = \gamma_0^{-1}$ (dashed green) and the population of the state $|a_2\rangle$ remains zero. On the other hand, when the atom is located at the focus of the metasurface, it experiences an AQV which induces quantum interference among the decay channels $|a_{1,2}\rangle \rightarrow |b\rangle$. Subsequently the decay of the excited state $|a_1\rangle$ is suppressed (dashed red) and we see non-zero population transfer to $|a_2\rangle$ (solid red). At initial times, the evolution of the population of the state $|a_2\rangle$ is $\varrho_{a_2 a_2}(t) \approx (|\kappa_1|^2/4)t^2$ while the coherence grows linearly as $\varrho_{a_1 a_2} \approx (\kappa_1^*/2)t$. In Fig. 5(b) we have plotted the transient coherence (real part of $\varrho_{a_1 a_2}$) at different points in space along the z-axis. Non-zero coherence, along with non-zero population in the state $|a_2\rangle$, is a clear signature of vacuum-induced cross-damping between the two transitions $|a_{1,2}\rangle \leftrightarrow |b\rangle$. Vacuum induced coherence effects can also be probed by studying resonance profiles[43], photon-photon correlation[44], etc.

A viable way to place and hold quantum emitters at remote distances from the plasmonic meta-surface is by trapping ultra-cold atomic gases in optical latices or atomic chips. For instance, trapping a Bose-Einstein condensate (BEC) at ~ 5 micron from a gold wire has been success-fully demonstrated in [45]. By contrast, trapping below or at sub-micron distances from a metallic interface is often challenging owing to fluctuating spatial and temporal magnetic fields, surface tunneling, Casimir-Polder (CP) forces, thermal noise, etc.[10]. A possibility of trapping an ultra-cold atom at sub-micron dimensions near a wire has been proposed in[46]. However, although metallic interfaces can induce strong anisotropic quantum vacuum at distances $d \ll \lambda_0$, precise control over positioning and holding atoms within this limit is extremely difficult if not impossible. Hence, creating a strong AQV at distances $d \gg \lambda_0$ is indeed necessary for viable experimental demonstrations. We anticipate that our approach will not only bridge the gap between plasmonic metasurfaces and QED[47] but also open a door for engineering light-matter interactions with single or no photons, constructing long-range interaction between quantum emitters, and exploring fundamental quantum physics.

should be addressed to X.Z. (xiang@berkeley.edu)

—————

[1] G. S. Agarwal, *Quantum Statistical Theories of Spontaneous Emission and Their Relation to Other Approaches*, edited by G. Mohler *et al.* Springer Tracts in Modern Physics: Quantum Optics Vol. 70 (Springer-Verlag, Berlin, 1974).

[2] M. O. Scully, K. R. Chapin, K. E. Dorfman, M .B. Kim, and A. Svidzinsky, Proc. Natl. Acad. Sci. U. S. A.**108**, 15097(2011)

[3] H.-R. Xia, C. Y. Ye, and S.-Y. Zhu, Phys. Rev. Lett. **77**, 1032(1996).

[4] M. V. G. Dutt, J. Cheng, B. Li, X. Xu, X. Li, P. R. Berman, D. G. Steel, A. S. Bracker, D. Gammon, S. E. Economou, R.-B. Liu, and L .J. Sham, Phys. Rev. Lett. **94**, 227403(2005).

[5] K. P. Heeg, H.-C. Wille, K. Schlage, T. Guryeva, D. Schumacher, I. Uschmann, K. S. Schulze, B. Marx, T. Kampfer, G. G. Paulus, R. Rohlsberger, and J. Evers. Phys. Rev. Lett. **111**, 073601(2013).

[6] G. S. Agarwal, Phys. Rev. Lett. **84**, 5500(2000).

[7] V. Yannopapas, E. Paspalakis, and N. V. Vitanov, Phys. Rev. Lett. **103**, 063602(2009).

[8] Y. Gu, L. Wang, P. Ren, J. Zhang, T. Zhang, O. J. Martin, and Q. Gong, Nano Lett. **12**, 2488(2012).

[9] G.-X. Li, F.-L. Li, and S.-Y. Zhu, Phys. Rev. A **64**, 013819(2001).

[10] J. Reichel and V. Vuletic, editors, *Atom Chips*, Wiley-VCH, Weinheim, Germany, 2011.

[11] D. E. Chang, A. S. Sorensen, P. R. Hemmer, and M. D. Lukin, Phys. Rev. Lett. **97**, 053002(2006).

[12] D. E. Chang, J. D. Thompson, H. Park, V. Vuletic, A. S. Zibrov, P. Zoller, and M. D. Lukin, Phys. Rev. Lett.**103**, 123004(2009).

[13] Y. Yang, J. Xu, H. Chen, and S.-Y. Zhu, Phys. Rev. Lett. **100**, 043601(2008).

[14] J. Kastel and M. Fleischhauer, Phys. Rev. A **71**, 011804(R)(2005).

[15] A. Delga, J. Feist, J. Bravo-Abad, and F.J. Garcia-Vidal, Phys. Rev. Lett.**112**, 253601(1024).

[16] K. E. Dorfman, P. K. Jha, D. V. Voronine, P. Genevet, F. Capasso, and M. O. Scully, Phys. Rev. Lett. **111**, 043601(2013).

[17] P. K. Jha, X. Yin, and X. Zhang, Appl. Phys. Lett. **102**, 091111 (2013).

[18] G. S. Agarwal and S.-A. Biehs, Opt. Lett. **38**, 4421(2013).

[19] P. W. Milonni, *The Quantum Vacuum: An Introduction to Quantum Electrodynamics*, (New York: Academic Press 1994).

[20] A. V. Kildishev, A. Boltasseva, and V. M. Shalaev, Science **339**, 1232009(2013).

[21] N. Yu, F. Capasso, Nature Mater.**13**, 139(2014).

[22] N. Fang, H. Lee, C. Sun, and X. Zhang, Science **308** 534(2005).

[23] N. Yu, P. Genevet, M. A. Kats, F. Aieta, J.-P. Tetienne, F. Capasso, and Z. Gaburro, Science **334**, 333(2011).

[24] X. Ni, N. K. Emani, A. V. Kildishev, A. Boltasseva, and V. M. Shalaev, Science **335**, 427(2012).

[25] N. Shitrit, I. Yulevich, E. Maguid, D. Ozeri, D. Veksler, V. Kleiner, and E. Hasman, Science **340**, 724(2013).

[26] X. Yin, Z. Ye, J. Rho, Y. Wang, and X. Zhang, Science **339**, 1405(2013).

[27] S. Sun, Q. He, S. Xiao, Q. Xu, X. Li, and L. Zhou, Nat. Mater. **11**, 426(2012).

[28] F. Aieta, P. Genevet, M. A. Kats, N. Yu, R. Blanchard, Z. Gaburro, and F. Capasso, Nano Letters 12, 4932 (2012).

[29] X. Ni, A. V. Kildishev, and V. M. Shalaev, Nat. Commun. **4**, 2807(2013).

[30] J. Lee, M. Tymchenko, C. Argyropoulos, P. Y. Chen, F. Lu, F. Demmerle, G. Boehm, M. C. Amann, A. Alu, and M. Belkin , Nature **511**, 65(2014).

[31] A. Silva, F. Monticone, G. Castaldi, V. Galdi, A. Alu, and N. Engheta, Science **343**, 160(2014).

[32] R. Fleury, D. L. Sounas, and A. Alu, Phys. Rev. Lett. **113**,023903(2014).

[33] R. Folman, P. Krüger, J. Schmiedmayer, J. Denschlag, and C. Henkel, Adv. At. Mol. Opt. Phys. **48**, 263(2002).

[34] S. Sun, K.-Y. Yang, C.-M. Wang, T.-K. Juan, W. T. Chen, C. Y. Liao, Q. He, S. Xiao, W. -T. Kung and G.-Y. Guo, Nano Lett.**12**, 6223(2012).

[35] A. Pors, O. Albrektsen, I. P. Radko, and S. I. Bozhevolnyi, Sci. Rep. **3**, 2155(2013).

[36] See Supplemental Material at [url] for details of equation of motion of the quantum emitter (three-level atom in V-configuration) and calculation of reflection efficiency. It also includes Refs.[37–41].

[37] P. B. Johnson and R. W. Christy, Phys. Rev. B **6**, 4370 (1972).

[38] D. A. Cardimona., M. G. Raymer, and C. R. Stroud Jr., J. Phys. B **15**, 55 (1982).

[39] P. Zhou, and S. Swain, Phys. Rev. Lett., **78**, 3995 (1996).

[40] H. T. Dung, S. Y. Buhmann, L. Knoll, D.-G. Welsch, S. Scheel, and J. Kastel, Phys. Rev. A **68**, 043816(2003).

[41] G. S. Agarwal and A. K. Patnaik, Phys. Rev. A 63, 043805(2001).

[42] L. Novotny and B. Hecht, *Principles of Nano-Optics* Cambridge University Press: Cambridge, U.K., 2006.

[43] K. E. Dorfman, P. K. Jha, and S. Das, Phys. Rev. A 84, 053803 (2011).

[44] S. Das and G. S. Agarwal, Phys. Rev. A **77**, 033850(2008).

[45] S. Wildermuth, S. Hofferberth, I. Lesanovsky, E. Haller, L. M. Andersson, S. Groth, I. Bar-Joseph, P. Kruger, and Nature **435**, 440(2005).

[46] R. Salem, Y. Japha, J. Chab, B. Hadad, M. Keil, K. A. Milton, and R. Folman, New J. Phys.**12**, 023039(2010).

[47] J. D. Thompson, T. G. Tiecke, N. P. de Leon, J. Feist, A. V. Akimov, M. Gullans, A. S. Zibrov, V. Vuletic, M. D. Lukin, Science **340**, 1202(2013).
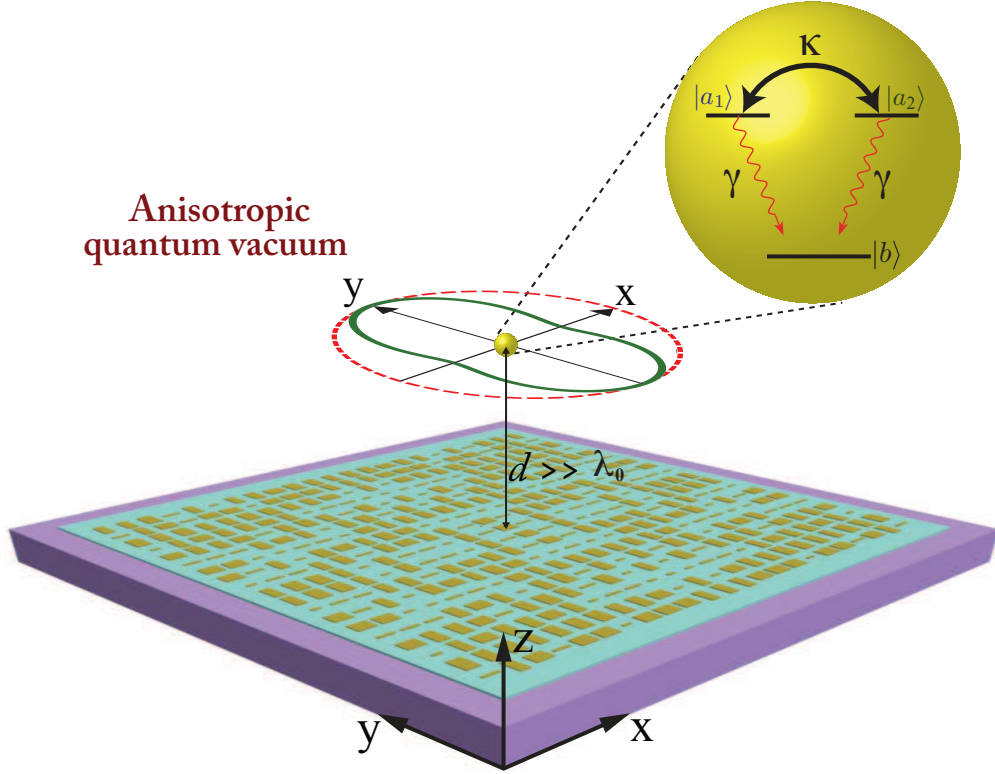
FIG. 1. (color online) Metasurface-enabled macroscopic quantum vacuum engineering. The metasurface creates a strong AQV in the vicinity of a quantum emitter at some macroscopic distance d. Decay of an in-plane, linear dipole is anisotropic (solid green curve) with respect to an isotropic quantum vacuum with no physical boundary (dashed red line). The inset shows a three-level atom, at some macroscopic distance from the metasurface, with coupled orthogonal transitions $(\wp_{a_1 b} \cdot \wp_{a_2 b}^* = 0)$ whose coupling strength κ depends on the anisotropy of the quantum vacuum. Coherent coupling among the transitions is accomplished by exchanging *virtual photons* via the quantum vacuum. Such AQV induces QI among the decay channels.
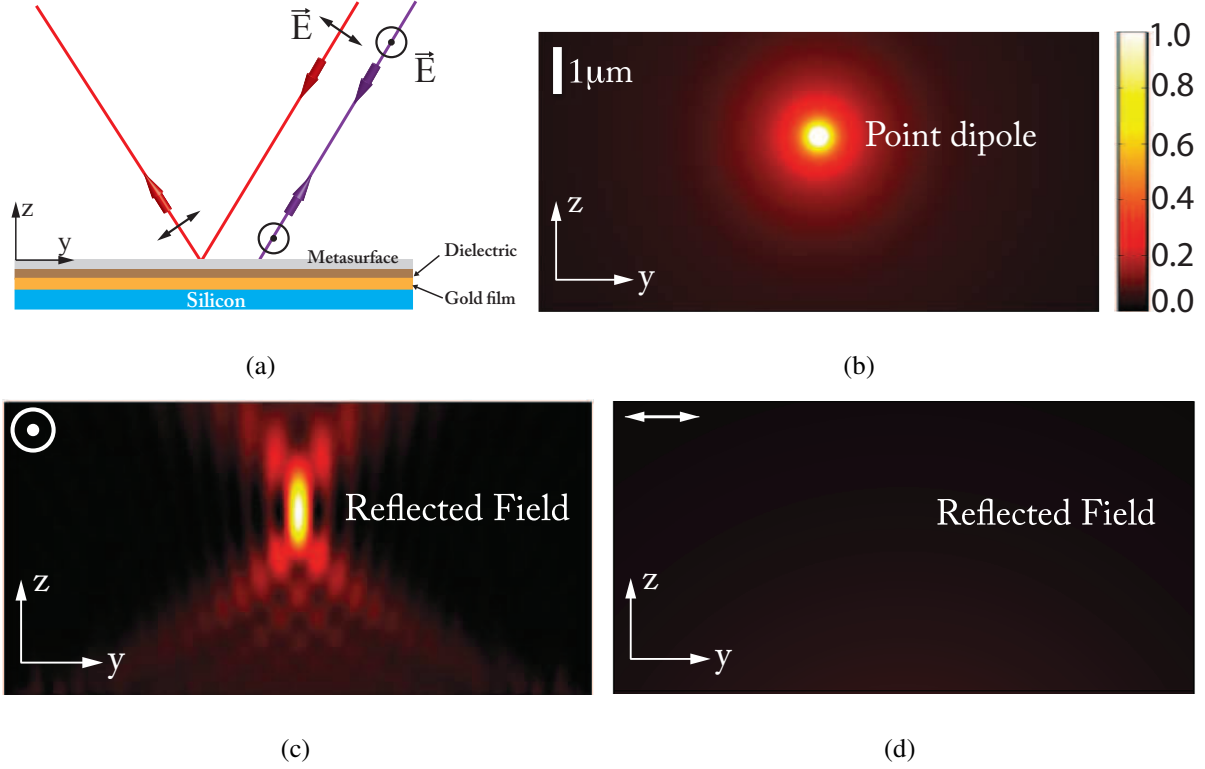
FIG. 2. (color online) Principle of metasurface-enabled remote anisotropic quantum vacuum. (a) Two-dimensional schematic illustration of polarization dependent response of the metasurface. Incident y-z polarized light is defocused by the metasurface while the x-polarized light is focused back to the source. (b) Simulated field intensity distribution from a linear dipole source. (c) Simulated field intensity distribution of the reflected field, above the metasurface, for the x-dipole. With an optimized design we achieved 81%, normalized to total field incident on the metasurface, reflection efficiency of the incident field back to the source. However for y-dipole the incident field is defocused and the corresponding reflected field intensity distribution is shown in (d). For all numerical simulations (b,c,d) the dipole is located at a distance of 3.7-micron from the metasurface with cross-sectional dimension (12μm $\times 12\mu$m).
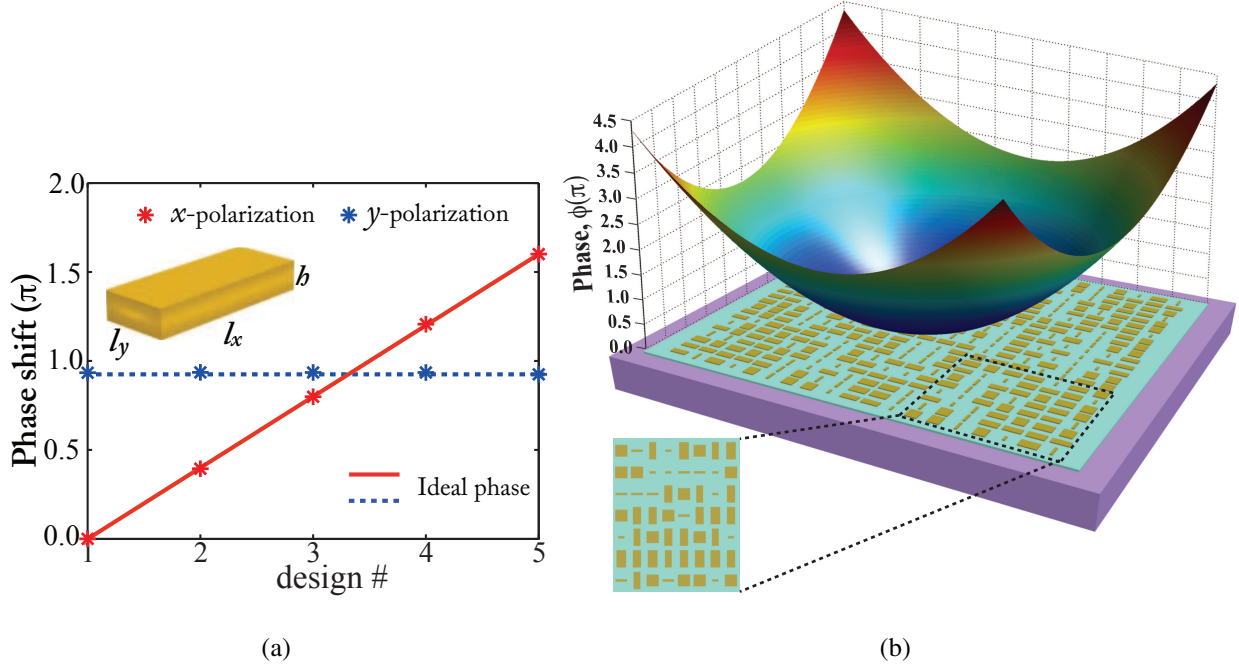
FIG. 3. (color online) Polarization dependent phase shift and vanishing optical path: (a) Phase shift imprinted by the five constitutional nano-antennas for the x-polarized (red stars) and y-polarized (blue stars) incident light. For the x-polarized light the response is linear and covers the full phase range 0 to 2π, and matches well with the required ideal phase indicated by the solid red line; while for the y-polarized light the corresponding phase shift for each constitutional nano-antenna is a constant. (b) Two-dimensional distribution of the phase profile required upon the reflection to focus the incident light and compensate the optical path length from a x-dipole to its image. The inset shows the top view of a small piece. The dimensions (l_x nm, l_y nm, 30 nm) of the five nano-antennas are: (32, 154), (144, 161), (166, 159), (186, 157), and (229, 153) respectively.
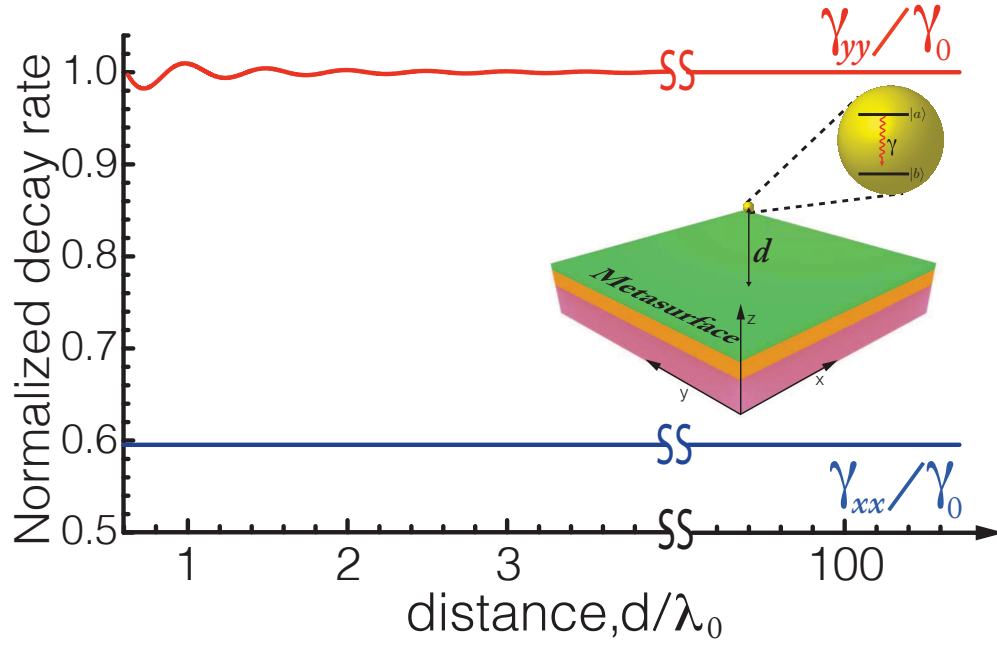
FIG. 4. (color online) Anisotropic decay rate of a quantum emitter over remote distances: Plot of the normalized decay rate of a x-dipole(blue line) and y-dipole (red line) located at the focus of the metasurface against distance d/λ_0. As the distance between the x-dipole and the mestasurface is increased (along the z-direction) the decay rate does not change and remains flat. However, for y-dipole the decay rate oscillate and quickly goes to the value of $\gamma_{yy} = \gamma_0$ and remains constant thereafter. We can induce an AQV in x-y plane i.e $\gamma_{xx} \neq \gamma_{yy}$ over remote distances by designing the surface for each point along the z-axis.
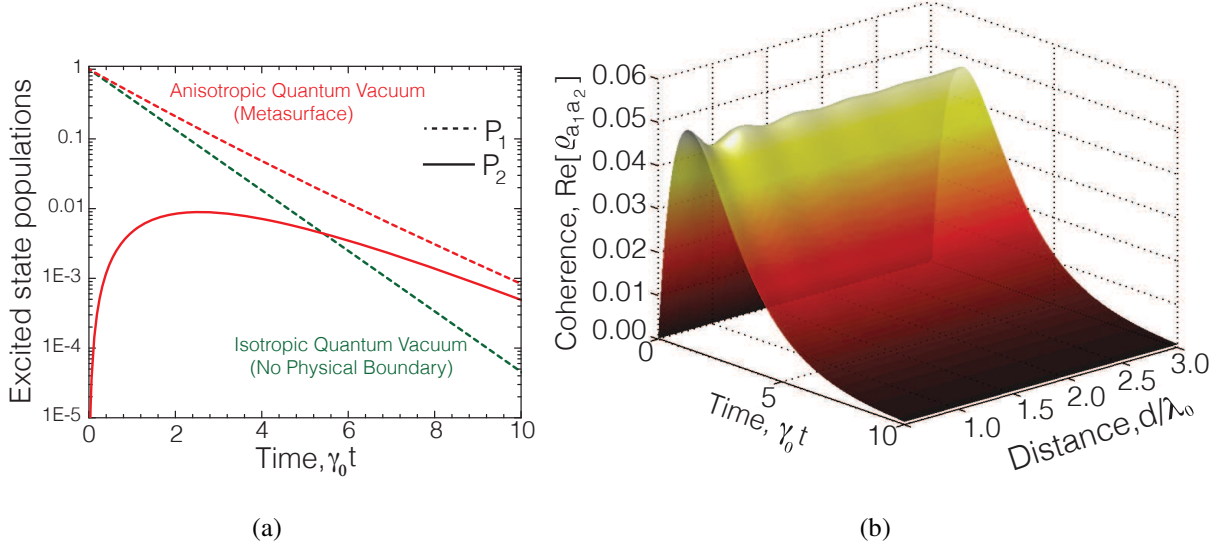
FIG. 5. (color online) Anisotropic quantum vacuum-induced quantum interference: (a) Plot of the excited state populations $P_i = \varrho_{a_i a_i}$ of a three-level atom (shown in Fig. 1 inset) located at $20\lambda_0$ distance from the metasurface, initially prepared in $|a_1\rangle$, as a function of normalized time $\gamma_0 t$. In an isotropic quantum vacuum, with no physical boundary ($\kappa = 0$) the atom decays exponential (dashed green) with time constant γ_0^{-1} and the population of the state $|a_2\rangle$ remains zero. On the other hand, when the atom is located at the focus of the metasurface the decay of the excited state $|a_1\rangle$ is suppressed (dashed red) and a non-zero population transfer to the level $|a_2\rangle$ (solid red). (b) 3D-Plot of the transient coherence ($\text{Re}[\varrho_{a_1 a_2}]$) between the excited states as a function of normalized time ($\gamma_0 t$) and distance (d/λ_0). Non-zero coherence, is a clear signature of vacuum-induced cross damping, can be sustained over macroscopic distances